AIAA 96-0486

Electrostatic Charging of the Pathfinder Rover

Mark W. Siebert
University of Toledo
Toledo, OH

Joseph C. Kolecki
NASA Lewis Research Center
Cleveland, OH

34th Aerospace Sciences Meeting & Exhibit
January 15-18, 1996 / Reno, NV

ELECTROSTATIC CHARGING OF THE PATHFINDER ROVER

Mark W. Siebert
University of Toledo
Toledo, OH

Joseph C. Kolecki
NASA Lewis Research Center
Cleveland, OH

ABSTRACT

The Mars Pathfinder mission will send a lander and a rover to the martian surface. Because of the extremely dry conditions on Mars, electrostatic charging of the rover is expected to occur as it moves about. Charge accumulation may result in high electrical potentials and discharge through the martian atmosphere. Such discharge could interfere with the operation of electrical elements on the rover.

A strategy was sought to mitigate this charge accumulation as a precautionary measure. Ground tests were performed to demonstrate charging in laboratory conditions simulating the surface conditions expected at Mars. Tests showed that a rover wheel, driven at typical rover speeds, will accumulate electrical charge and develop significant electrical potentials (average observed, 110 volts). Measurements were made of wheel electrical potential, and wheel capacitance. From these quantities, the amount of absolute charge was estimated. An engineering solution was developed and recommended to mitigate charge accumulation. That solution has been implemented on the actual rover.

INTRODUCTION

A free ranging, solar powered surface rover will be delivered to Mars as part of the Pathfinder mission. Pathfinder will be launched in December, 1996, and will land on Mars on July 4, 1997. The rover will travel about on the martian surface, conducting technology experiments and serving as an instrument deployment mechanism (Ref. 1). Because of the extremely dry

conditions on Mars, electrostatic charging of the rover is expected to occur as it moves about. Experiments conducted in a simulated martian environment at the NASA Lewis Research Center have shown that a rover wheel, driven at typical rover speeds, will accumulate electrical charge on the order of 8×10^{-9} C, and develop electrical potentials averaging 110 V with transients 2- to 3-times that value.

Voltages of 100 V and greater are believed sufficient to produce electrical discharge in the Martian atmosphere. Also, with an accumulated net charge of 8×10^{-9} C, and average arc time interval of 1 µs, arcs can occur with estimated arc currents reaching almost 10 mA. Discharges of this magnitude could interfere with the operation of sensitive electrical elements on the rover (Ref. 2, 3, 4).

In laboratory tests, a typical wheel was driven in Arizona Lunar Simulant (ALS). This material was chosen because of its availability (from NASA/JSC), and its relatively low outgasing rate, enabling chamber pumpdown to be accomplished within a single day. About a pound of the material was used.

When the wheel was driven at typical rover speeds (.76 - 1.5 cm/s) in the ALS, electrical charging occurred. The charge accumulated was determined by measuring the electrical potential of the wheel using a capacitively coupled electrostatic probe, and multiplying the result by the wheel capacitance (approximately 74 pico-farads). The charge is believed to arise during compaction of the ALS by the moving wheel.

To dissipate accumulated electrical charge, a metal point was attached to the wheel. On the average, the wheel without any point developed an average steady-state electrostatic voltage of 110 V. Adding a discharge point resulted in electrical potential reductions of up to 15 - 20% of the steady state value. The reduction in potential is believed due to the dissipation of image charge from conducting surfaces of the wheel. Charge connected with adherent dust grains bleeds off very slowly due to the low conductivity of the dust.

As a result of the tests conducted at Lewis, and recommendations made to JPL, the Pathfinder rover will incorporate small wire discharge points on the rover at the base of the rover antenna. This component is electrically continuous with the other parts of the rover.

EXPERIMENT DESCRIPTION

In December, 1993, a memo was sent to the Pathfinder Office at the Jet Propulsion Laboratory (JPL) which stated the result of a preliminary calculation made of rover potential and charging rate. While the calculation was only an estimate, it pointed to

possibilities that were of interest to the Pathfinder team. As a result of this communication, NASA Lewis was requested to perform laboratory tests to determine whether charging was a real issue, and whether it could be mitigated by addition of a discharge point.

A Mars simulator facility had already been set up to conduct tests for the Wheel Abrasion Experiment (WAE, Ref. 5). This facility was adapted to examine the problem of electrostatic charging. A capacitively coupled electrostatic probe was installed, and tests were run with a simulated Mars surface atmosphere and Arizona Lunar Simulant (ALS). Experiments were conducted with two different wheels, hereafter referred to as the test wheel and the System Integration Model (SIM) wheel. The test wheel was a crude mock-up of the rover wheel, made to approximate dimensions. The SIM wheel was a more detailed model of the flight wheel. Both were driven at typical rover speeds. Charging was found to occur.

The rover wheel, driven at typical rover speeds, accumulated an electrical charge of about 8×10^{9} C, and developed electrical potentials on the order of 110 V with transients 2- to 3- times that value.

Facility Description

The Mars simulator facility is a 62 cm diameter by 62 cm long vacuum chamber. For charging tests, the chamber was initially pumped to a background pressure of 8×10^{-6} torr, then filled with Martian atmospheric simulant (approximate composition: 0.03% water, 0.153% carbon monoxide, 0.336% oxygen, 1.36% argon, 2.52% nitrogen, and balance carbon dioxide) to a pressure of 7 mbar. The wheel was mounted in a rotary tray filled to a depth of 15 mm with ALS, and driven with a variable-speed motor, external to the chamber. A xenon arc lamp provided a collimated light source to the wheel through a quartz window. A computer connected to an analog-to-digital converter continuously recorded data during the tests. (Fig. 1).

Procedure

The test wheels were run at speeds of 0.6 to 5.4 rpm. (The speed of the flight unit rover wheel on Mars will be 0.6 to 1.2 rpm). All outputs from wheel diagnostics were recorded. Test duration was typically ≥ 1000 s. The electrostatic probe was initially zeroed to chamber ground prior to each test, then repositioned and held perpendicularly to the wheel at 2 mm during the test. All tests were conducted at room temperature, 23 °C.

Two different wheels were used: the test wheel and the SIM wheel. Two types of discharge points were attached to each of the wheels: a 12.7 μm radius stainless steel wire cut at the end, and a tungsten wire electromachined at its end to a point of radius 1 μm (Fig. 2).

For the test wheel, the 12.7 μm stainless steel point and the tungsten point were soldered to a braided copper wire. The braided copper wire was wrapped around the wheel and held down with Kapton tape. The braided copper wire with the discharge point was brought to the wheel axle, and extended outward 5 cm. (Fig. 3).

For the SIM wheel, the tungsten and 12.7 μm steel points were soldered to a copper wire. The copper wire was held in contact with the wheel by one of the cap screws on the rim. The copper was brought to the wheel axle, and extended 5 cm as before.

RESULTS AND DISCUSSION

Mechanisms assumed responsible for wheel charging included dust compaction, and friction of the wheel in the ALS. These assumptions were tested in simple experiments.

1. The wheel axle was deliberately jarred while the wheel was charged. Large quantities of dust were observed to fall from the wheel, and the potential immediately dropped from 70 V to < 12 V.

2. A braking force was applied to the tray increasing slippage of the wheel from a nominal 10% to close to 100% in the ALS. No substantial changes in potential were noted.

3. The weight of the wheel was changed. Electrostatic charging was measured with and without a counterbalance. (In its usual configuration, the wheel was counterbalanced to a net load of 500 gm, the weight on one wheel of the rover in Mars gravity. When the counterbalance was removed, the load on the wheel increased to 1588 gm.) A 20% increase in wheel electrical potential was observed with the higher load.

These simple experiments implied that the dominant mechanism of charge generation was associated with dust compaction. Small grains assumed a positive charge, larger grains, a negative charge. The smaller grains were light enough to adhere to the wheel surface, and carried their net positive charge with them. The electrostatic probe registered the corresponding electrical potential. The entire metal surface of the wheel became charged through image charge generation. The addition of a point removed some of the image charge, allowing the wheel potential to drop proportionally. The track behind the moving wheel became charged with an equal charge of opposite sign. This charge was also observed with the electrostatic probe.

Test Wheel

A plot of electric potential vs. time for the test wheel is shown in Fig. 4. The initial transients and the steady state

region are labeled. These data were taken with no discharge point on the wheel. The potential settles to its steady-state value within six revolutions.

Comparison of the steady-state potentials with no discharge point, a 12.7 μm stainless steel discharge point, and the tungsten point are shown in figs. 5. Each of the two types of points produced about the same reduction in voltage. Increasing the number of 12.7 μm radius stainless steel points from 1 to 7 gave no further reduction in potential.

The effects of wheel loading and of adding a discharge point to the wheel are shown in Fig. 6. A wheel with a load of 500 gm and seven 12.7 μm radius stainless steel discharge points shows a reduction in steady-state potential by 14%[1] over a wheel with no point at comparable speeds. Retaining the seven points on the wheel, and increasing the wheel load from 500 gm to 1588 gm produced an increase in steady state potential by 16%. With no discharge point, increasing the wheel load from 500 gm to 1588 gm increased the steady state voltage by 25% at similar speeds.

A very slight dependence of voltage on wheel speed is also seen in Fig. 6.

---

[1] Percentages quoted are obtained by averaging over all data points.

SIM Wheel

The steady-state potentials of the test wheel, with 500 gm load, no discharge point, a 12.7 μm stainless steel point, and a tungsten point are shown in Fig. 7. The initial voltage transient of the wheel may be as large as three times the steady-state voltage. The reason for this transient is not clear. A chamber related effect might be the most reasonable first assumption. But since demonstrating rover charging and possible mitigation schemes were the primary objectives of these tests, and since time was short, a good deal of additional science was left undone.

Discharge Curves

The SIM wheel was initially charged by running it in the ALS. The wheel was then stopped and allowed to discharge into the test environment. Wheel potential was recorded during discharge. The resulting data were fitted to a decaying exponential and time constants were inferred. These time constants are:

3555±430 s, no discharge point
2898±386 s, 12.7 μm point
2553±340 s, 1 μm point

Data are averaged over the range of speeds, 0.6 to 5.4 rpm. Comparison with the case of no point shows that the time constant is lower by ≈20% when either the 1 μm or the 12.7 μm discharge point is present. The

discharge points have a significant effect on discharge rate of wheel.

Dust Charging

The negative charge left behind by the SIM wheel after its passage over the ALS was measured with the electrostatic probe appropriately repositioned. This charge was recorded for all three point configurations of points (above), and different wheel speeds. Results are shown in Fig. 8. The dust charged negatively to approximately the same absolute value of potential as the wheel. Grain size measurements (see below) showed that small grains adhered to the wheel, large grains did not. The negative values of the ALS potential reveal the charge separation between these differently sized grains.

Electron Microscopy of Arizona Lunar Simulant

The scanning electron microscope was used to determine the size and the shape distributions of the Arizona Lunar Simulant. Energy Dispersive X-ray Analysis (EDX) spectra were also taken to confirm its chemical composition. A typical EDX spectrum, with elemental peaks labeled, is shown in Fig. 9. (The Au peak is due to a 200 Å thick sputter coating to discharge the ALS particle surfaces). Electron microscope photographs were taken of the material that adhered to the wheel. The average grain diameter of the simulant that adhered to the wheel is on the order of

20 μm (Fig. 10 a), compared to the 100 μm of the bulk sample (Fig. 10 b).

Capacitance of SIM wheel

The capacitance of the SIM wheel (without the discharge point attached) was measured with the chamber backfilled with 7 mbar Martian atmosphere simulant and Arizona Lunar Simulant. A capacitance meter, with a range of 1 pF to 200,000 mF, was connected through an electrical feedthrough between the wheel and the chamber (ground). The capacitance of the wheel relative to the chamber, averaged over three sets of measurements, was found to be 74 pF. Thus at a mean potential of 110 V, the absolute charge of the wheel may be calculated as 8.1 X 10^{-9} C.

CONCLUSIONS

The tests reported indicate that the Pathfinder rover, in its traverses over the martian surface, may become sufficiently charged to raise its electrical potential to within the neighborhood of 110 V. Voltages of 100 V and greater are believed sufficient to produce electrical discharge in the Martian atmosphere. Also, with an accumulated net charge of 8 X 10^{-9} C, and average arc δt of 1 μs, arcs can occur with estimated arc currents reaching almost 10 mA. Discharges of this magnitude could interfere with the operation of sensitive electrical elements on the rover.

6

In the nominal mission on Mars, the rover will travel approximately two meters per day. During that time, the wheel will make at least five complete revolutions in the martian regolith. Experience with fine, dry clays in terrestrial laboratories demonstrates that charging is commonplace. It is not unreasonable to expect that the rover on Mars may charge more strongly than the wheel did in the laboratory. Discharges between active components, or between the rover and its surroundings may become very likely. Since actual martian conditions are unknown, discharge points will be added to the Pathfinder rover antenna base as a precaution against electrostatic charging. *Future missions should seriously consider including components to measure vehicle charging.* Possibilities might include an electroscope, or an optical means for detecting luminosity from electrical discharges taking place in and around the rover.

FINAL REMARK

During our investigation, the question arose whether a circuit model exists for charging/discharging the Pathfinder rover on Mars. Speculation is all that is possible at the moment. The rover will accumulate its charge from surface dust, then deliver some of that charge into the atmosphere through a point with a high electric field. Dust blowing by the rover in the martian surface wind will accumulate this charge and eventually fall back to the martian surface completing a circuit loop. The closest analogy is a Van de Graff generator in which the moving rover is the source of static charge, the point is the brush, the wind blown dust is the belt, and the martian surface to which the dust eventually returns is the accumulator. Perhaps an analog circuit model of this mechanism may be developed once more is known of the electrical characteristics of the actual martian surface material that will be encountered.

REFERENCES

1. "Mars Pathfinder Fact Sheet, Mission Summary", October 20, 1994, JPL 400-538.

2. Haberle, R. M. and Greeley, R. "Sand and Dust on Mars", NASA CP 10074, February, 1991, pg. 39.

3. Hillard, G. B. and Kolecki, J. C., "The Interaction of High Voltage Systems with the Environments of the Moon and Mars", NASA TM 106107, AIAA-93-0704, January, 1993.

4. Kolecki, J. C. and Hillard, G. B., "Electrical and Chemical Interactions at Mars Workshop, Final Report, Parts 1 and 2", NASA CP 10093, November, 1991.

5. Layman, W. E, Matijevic, T. R., Mishkin A. M. and Sorota A. R., "Microrover and LMRE Technical Baseline", Feb. 6, 1995, JPL MPF ROVER DFM 93- 006S.

7
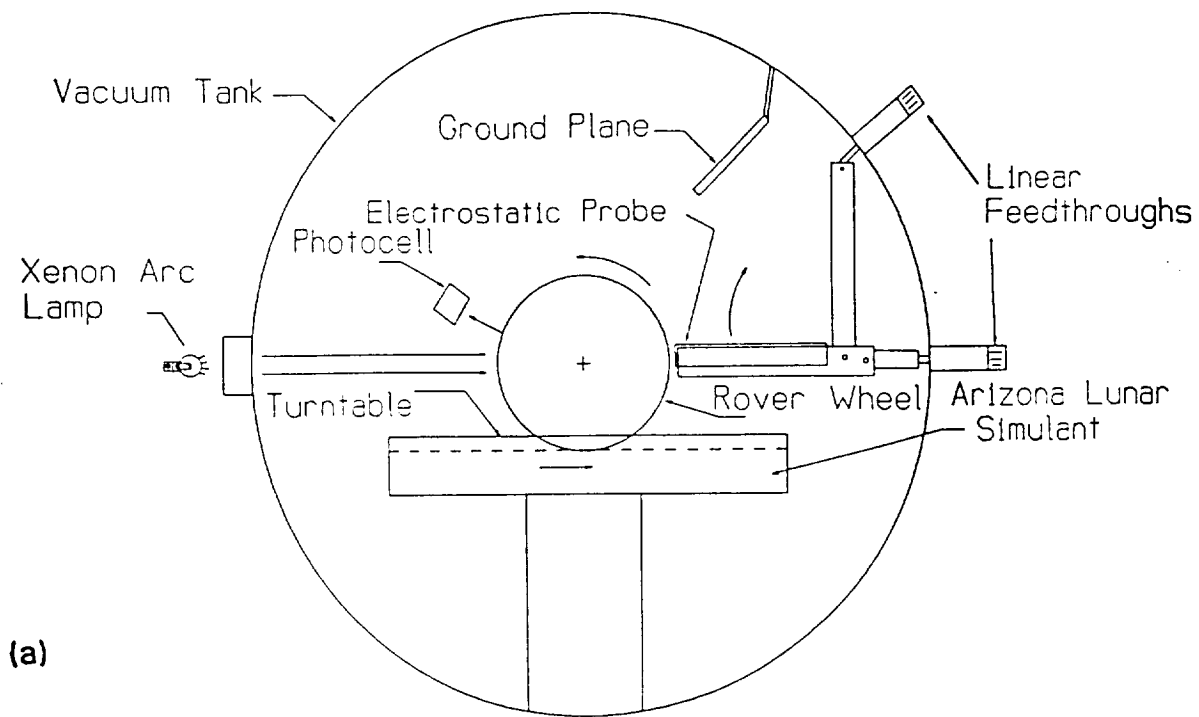
(a)
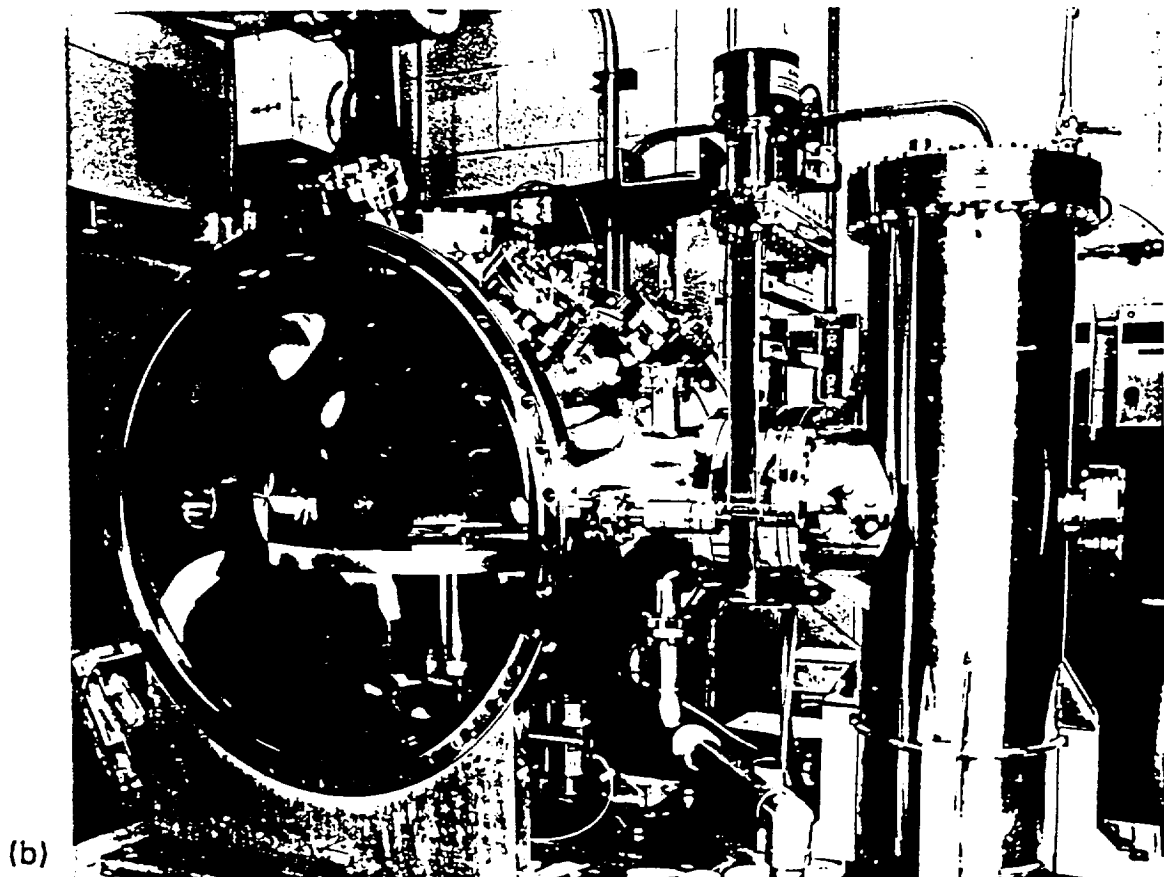
(b)
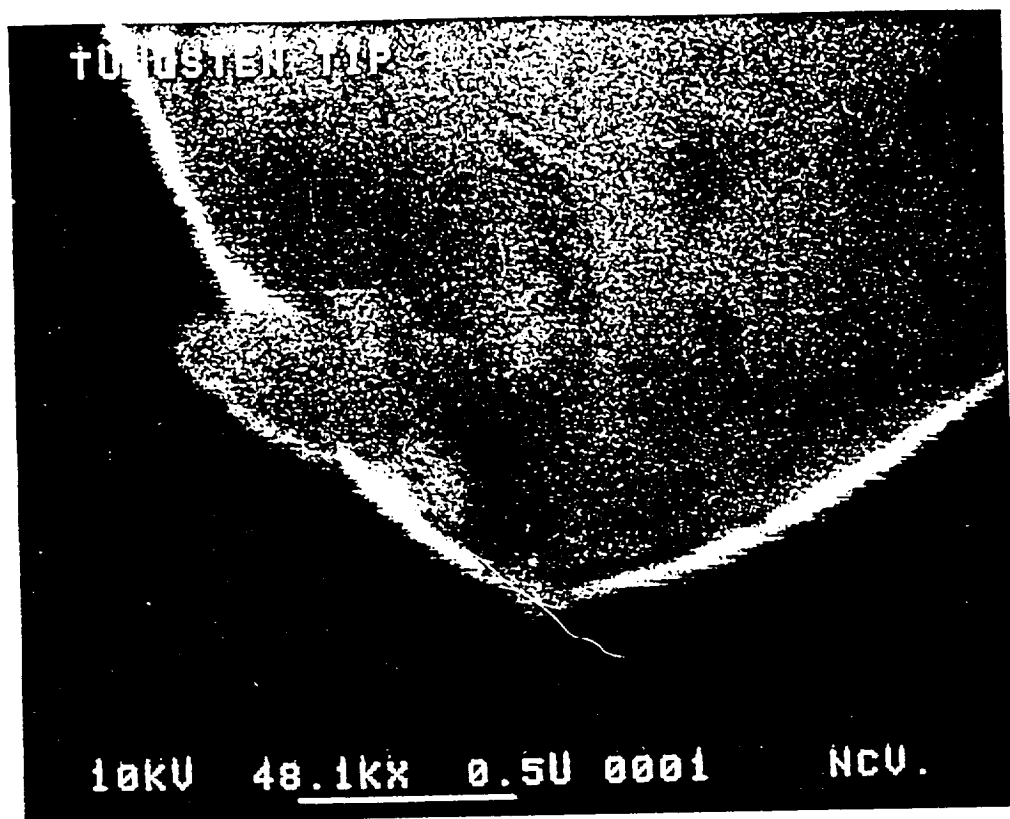
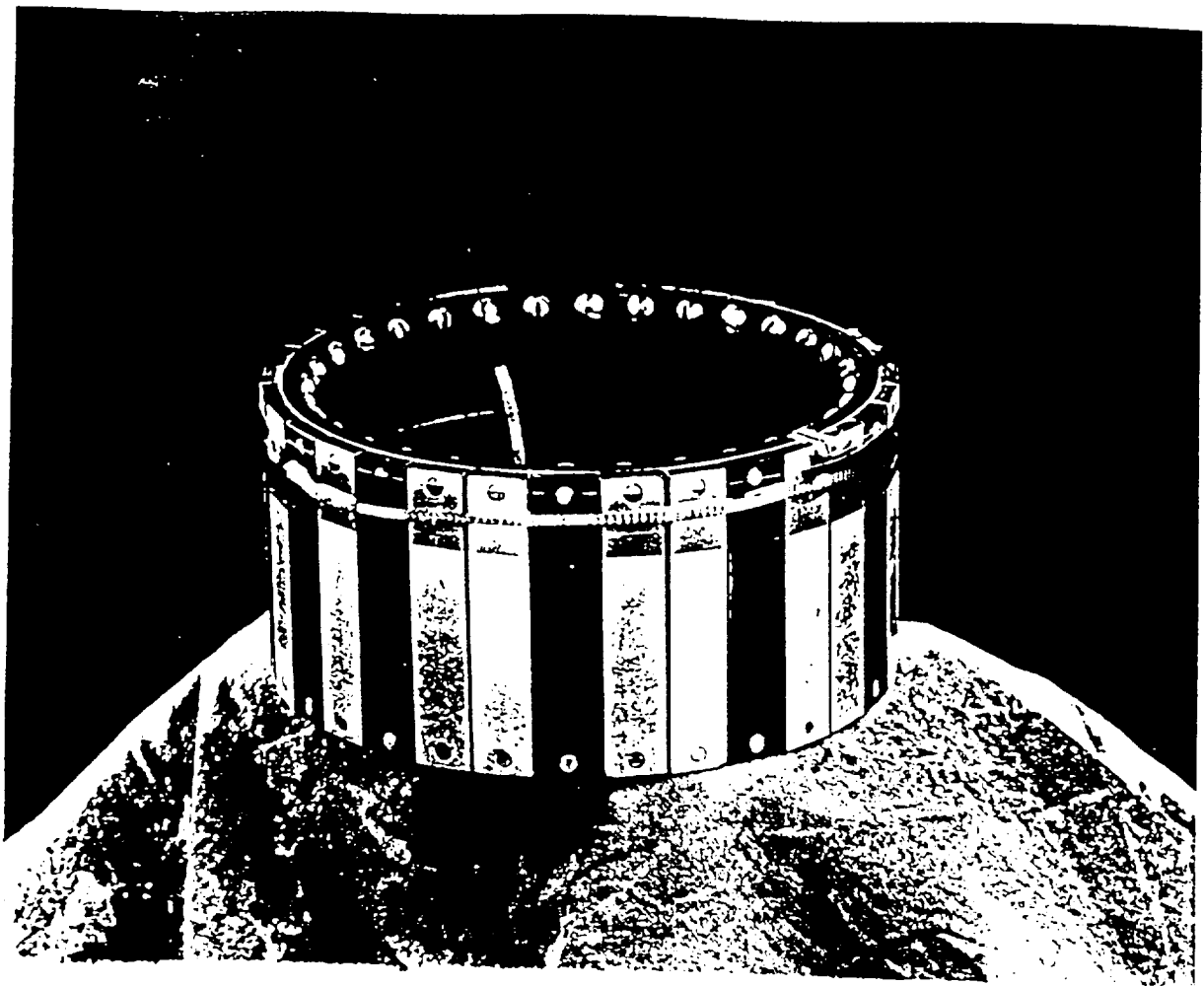Figure 1: Schematic (a) and photograph (b) of test facility

Figure 2: Electron microscope photograph of tungsten discharge point (scale on photo)
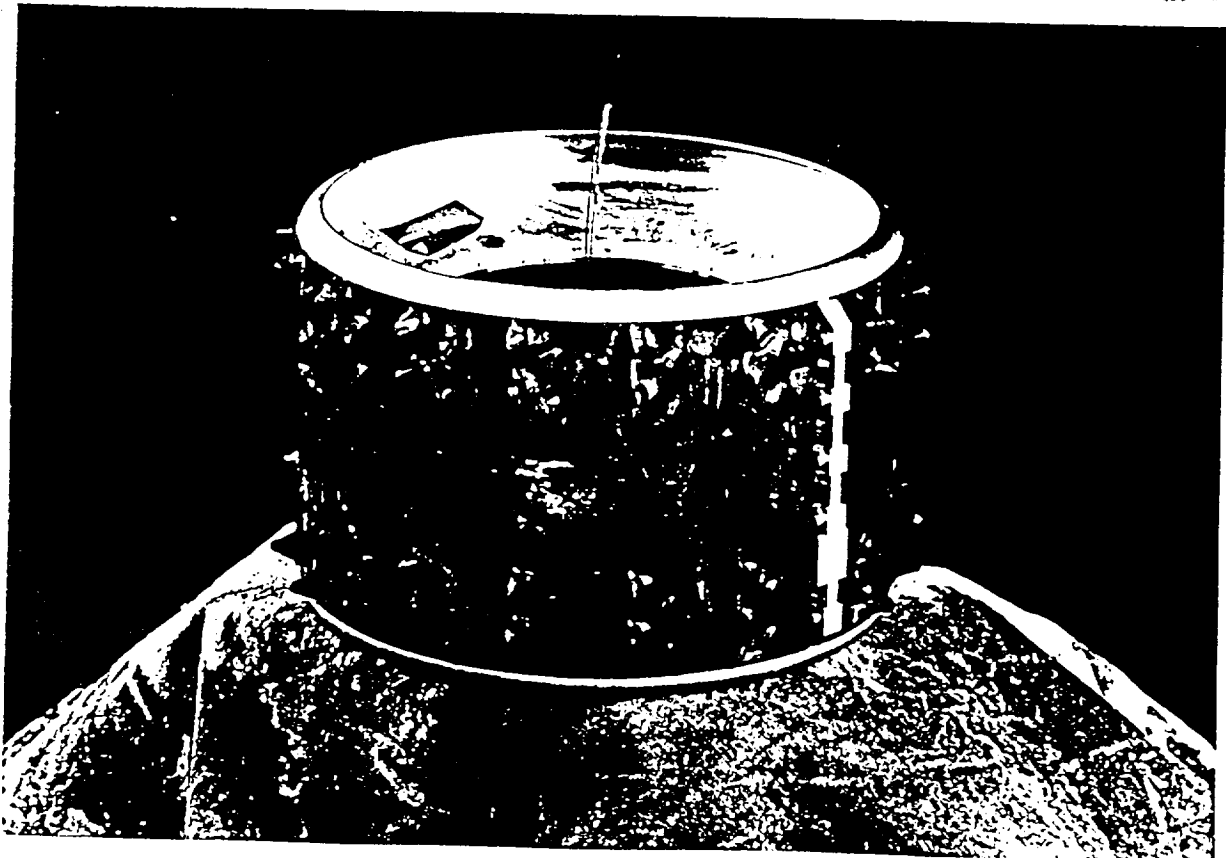
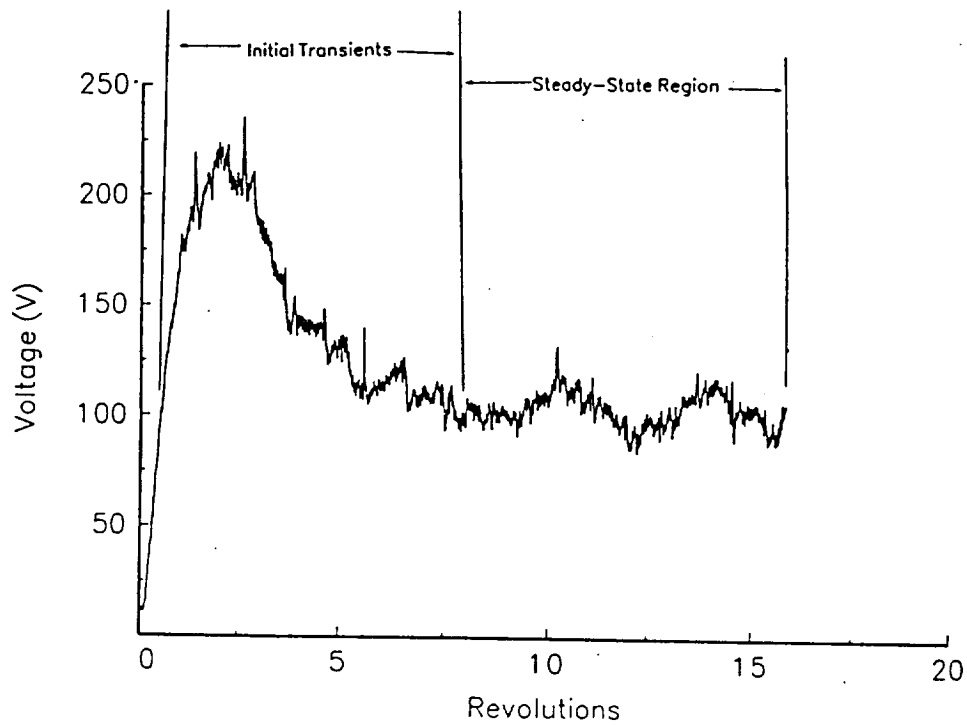Figure 3: Test Wheel (a); SIM Wheel (b)

Figure 4: Typical plot of test wheel potential as a function of number of revolutions (0.7 rpm, 500 gm load, ALS, 7 mbar martian atmosphere)
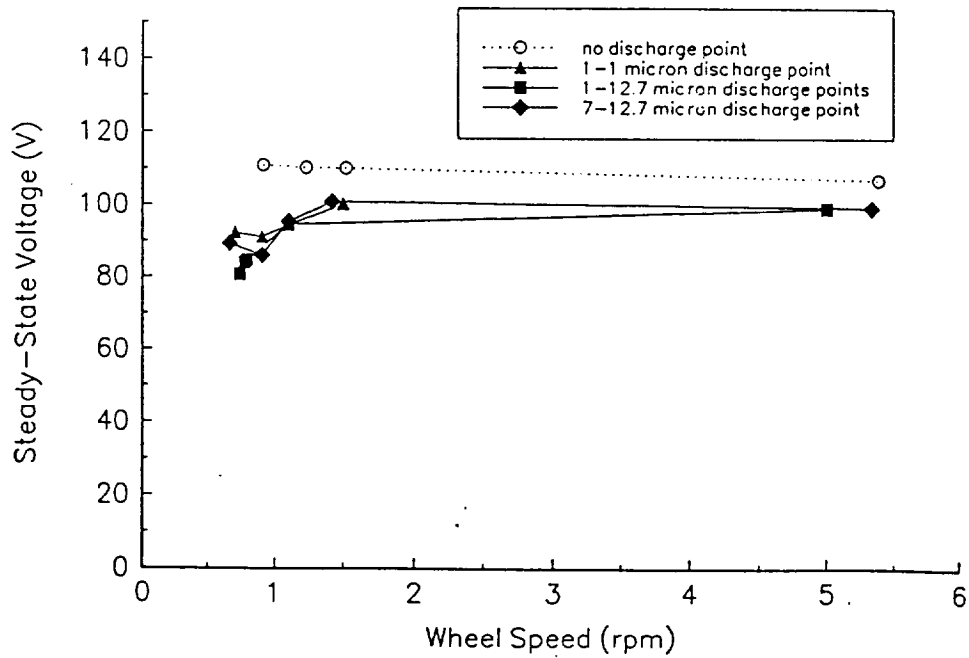

Figure 5: Dependence of test wheel steady state potential on type of discharge point (500 gm load)
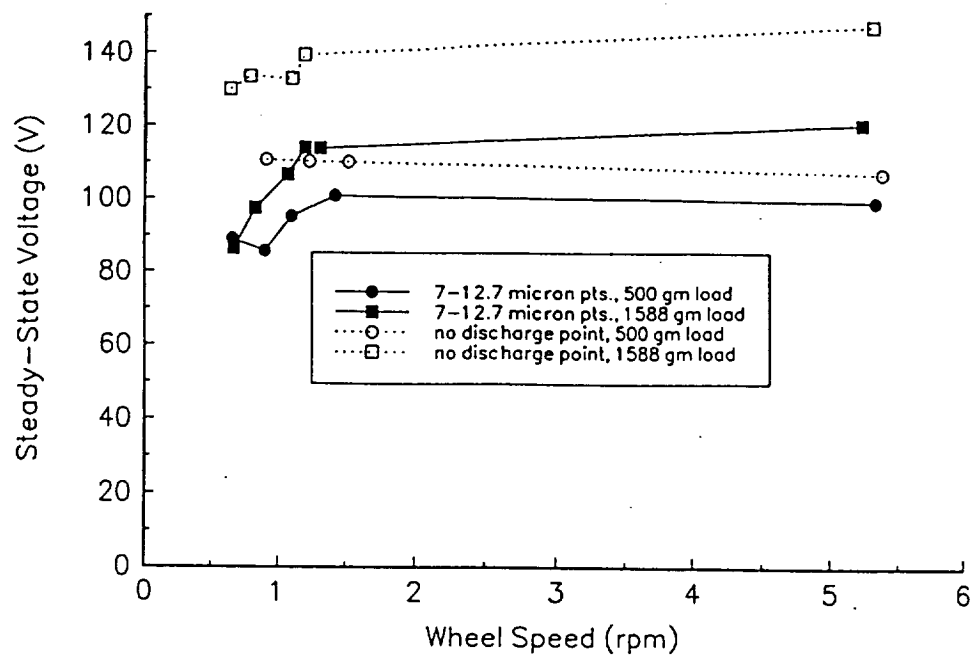
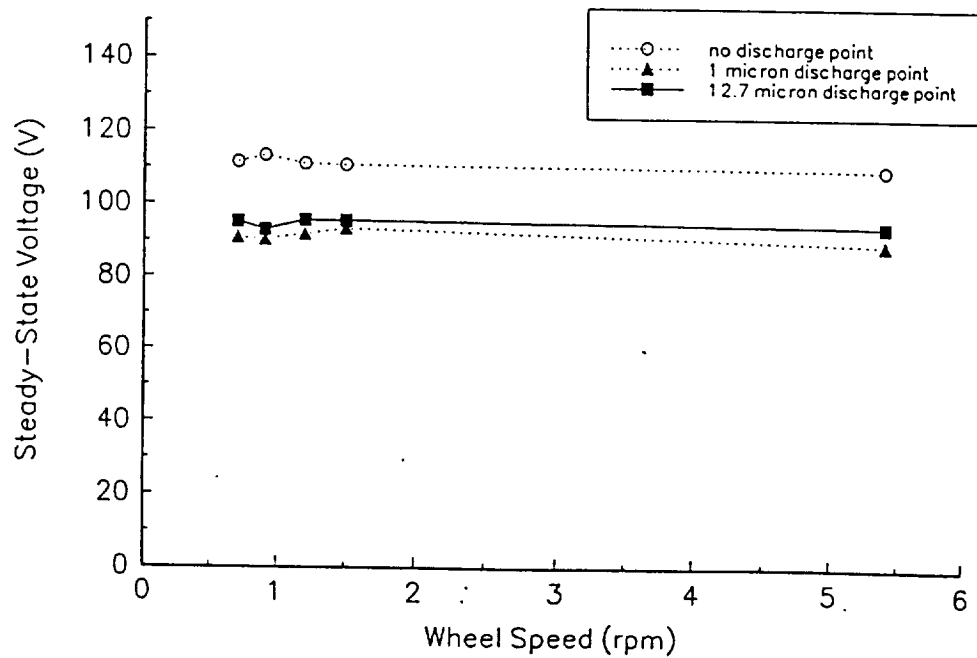**Figure 6: Dependence of test wheel steady state potential on load and type of discharge point**

Figure 7: Dependence of SIM wheel steady state potential on type of discharge point (500 gm load)

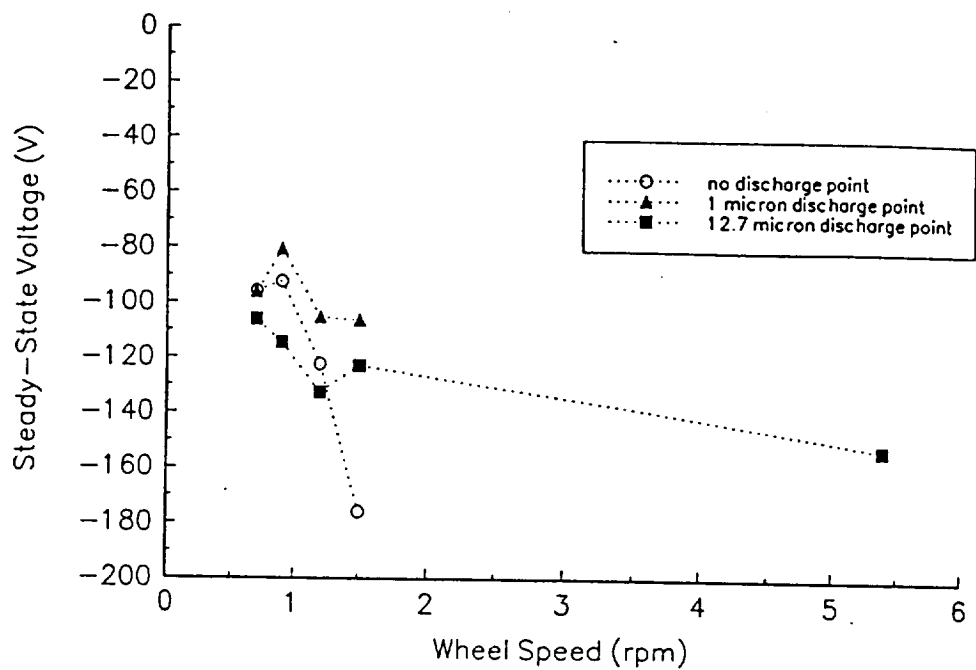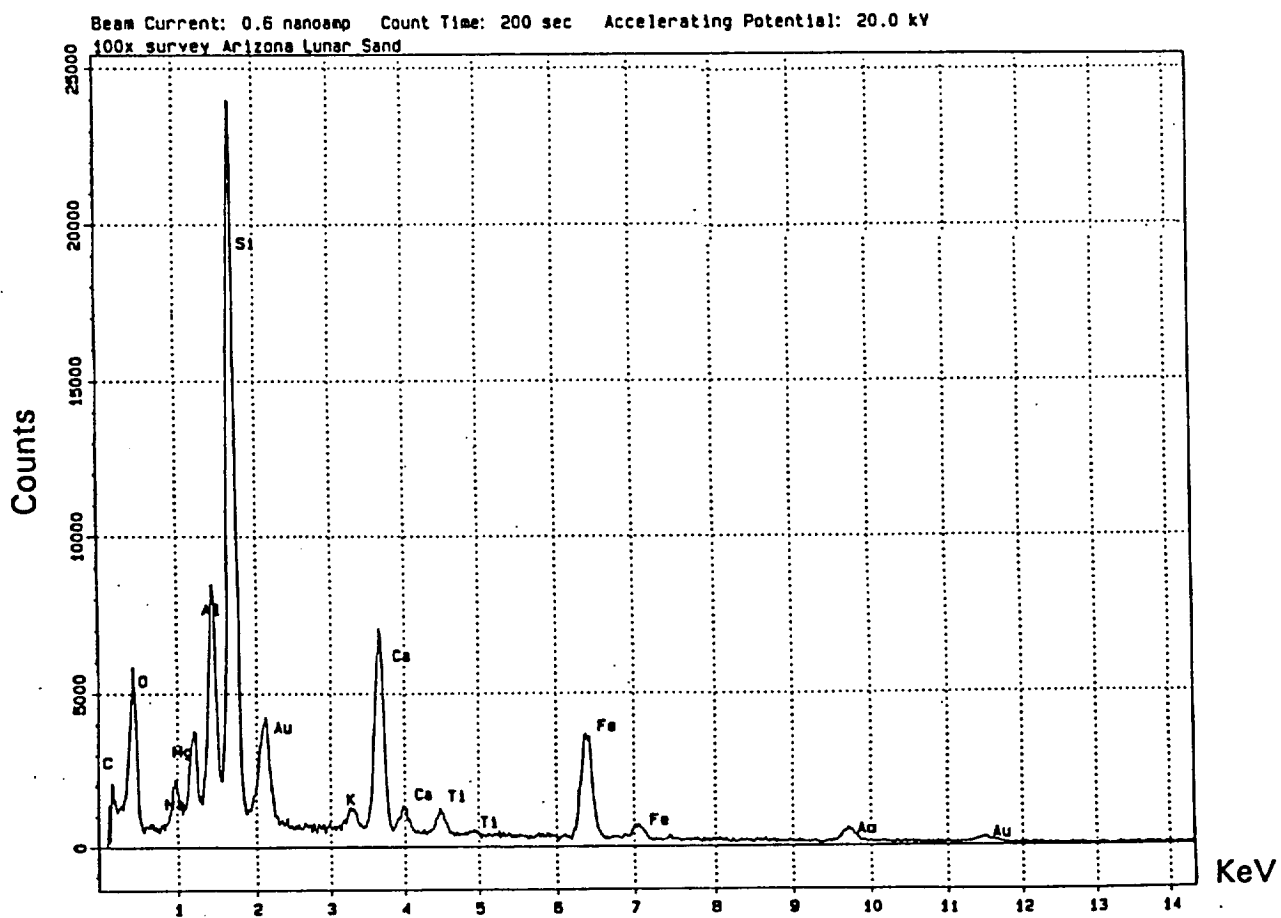Figure 8: ALS potential with SIM wheel and different discharge conditions

Figure 9: Energy Dispersive X-Ray Analysis of ALS

(a)

(b)

Figure 10: Electron microscope photographs of bulk ALS: (a) wheel track, (b) material collected off wheel

A New Antiwear Additive/Surface Pretreatment for PFPE Liquid Lubricants©

WILFREDO MORALES (Member, STLE) and ROBERT L. FUSARO (Fellow, STLE)
National Aeronautics and Space Administration
Lewis Research Center
Cleveland, Ohio 44135
MARK SIEBERT and THEO KEITH (Member, STLE)
University of Toledo
Toledo, Ohio 43606
and
RALPH JANSEN (Member, STLE) and PILAR HERRERA-FIERRO (Member, STLE)
Ohio Aerospace Institute
Cleveland, Ohio 44135

Pin-on-disk tribology experiments were conducted on a perfluoropolyalkylether (PFPE) liquid lubricant with and without a new PFPE lubricant antiwear additive material: a silane. It was found that the silane provided moderate improvement in the antiwear performance of the PFPE lubricant when applied to the metallic surface as a surface coating or when added to the PFPE as a dispersion (emulsion). Slightly better results were obtained by using the combination of a surface coating and an emulsion of the silane. The silane emulsions or coatings did not affect the friction properties of the lubricant. Micro-Fourier transformation infrared (μFTIR) spectroscopy analysis was performed to study silane transfer films and the degradation of the PFPE. The silane was found to mitigate degradation of the PFPE which may have been the major reason for the improved antiwear performance observed.

KEY WORDS

Lubricants, Antiwear Additives, Polyethers, Surface Analytical Techniques

INTRODUCTION

A class of high molecular weight liquid perfluoroethers, which were designated perfluoropolyalkylethers (PFPEs), was synthesized in the 1960s (*1*), (*2*). These liquids possessed excellent high temperature stability and low vaporization pressures and, thus, were immediately recognized to have potential for use in aerospace applications. While PFPEs have been used successfully as diffusion pump oils (*3*), dielectric fluids (*4*), and as lubricants (*5*), their potential as outstanding aerospace lubricants has not been realized. The main reason has been that they tend to decompose under boundary lubrication conditions, generating extremely reactive fluorinated products that can attack metal surfaces leading to increased wear and corrosion.

One method for mitigating PFPE decomposition is the use of soluble additives in the liquid lubricant, but the difficulty is that known additives for hydrocarbon-based liquid lubricants are not soluble in the PFPEs. This has led to studies (*6*), (*7*) investigating the use of highly fluorinated compounds as potential soluble additives for PFPEs. One possible drawback for the use of fluorinated additives is that many of these compounds have much lower vapor pressures than the PFPEs. Another drawback is that these additives may decompose, generating reactive fluorinated products.

Static thermal tests have shown that PFPEs decompose at elevated temperatures in the presence of certain metal oxides or metal fluorides, and it has been suggested that active Lewis acid sites on metal oxides or fluorides are responsible for PFPE catalytic decomposition (*8*)–(*10*). Recent studies, however, have indicated that Lewis acid sites may not be responsible for decomposition (*11*)–(*13*). For example, Ng et al. (*12*) observed that perfluorodiethylether decomposed on both untreated and pyridine-treated dehydroxylated aluminum oxide surfaces. Since pyridine is a compound widely used to block the action of Lewis acids, the results suggested that Lewis acid sites were not the reason for decomposition. Ng et al. also observed that perfluorodiethylether did not decompose on dehydroxylated alumina surfaces treated with a $(CH_3)_3$-SiCl vapor. They suggested that the following reaction took place which passivated (silylated) the alumina surfaces:

$$Al\text{-}OH + ClSi\text{-}(CH_3)_3 \rightarrow Al\text{-}O\text{-}Si(CH_3)_3 + HCl$$
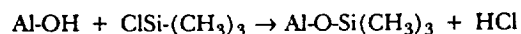
Morales (*13*) decomposed a commercial PFPE on both alpha and gamma alumina surfaces at and above 200°C. He

found that a pyridine treatment of the alumina surfaces did not prevent PFPE decomposition. He did observe, however, that by treating the surfaces of the alumina with various liquid silanes the decomposition of the PFPEs was mitigated. Surface treatment with one particular silane, 3-aminopropyltriethoxysilane, prevented decomposition up to 350°C.

The static decomposition studies by Ng et al. and Morales led to the idea of using a silane to minimize PFPE decomposition and the wear of the sliding surfaces under boundary lubrication conditions. To evaluate this concept, an experimental program was developed using a pin-on-disk tribometer to investigate the friction, wear and degradation of a PFPE oil under boundary lubrication conditions over short- and long-term sliding conditions. The silane was applied as a coating to the sliding specimens or as a dispersion (emulsion) to the PFPE liquid. Optical microscopy and micro-Fourier transformation infrared (µFTIR) microscopy examinations of the oil and surfaces were conducted to evaluate decomposition products.
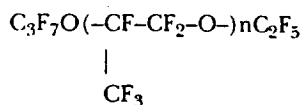
EXPERIMENTAL

Test Variables

To study the effect of a silane coating and/or emulsion on the friction, wear, and degradation properties of a PFPE oil, the following conditions were evaluated: silane emulsion, silane disk coating, silane disk and pin coatings, silane emulsion and silane disk coating, silane emulsion and pin and disk coatings, and no treatment.
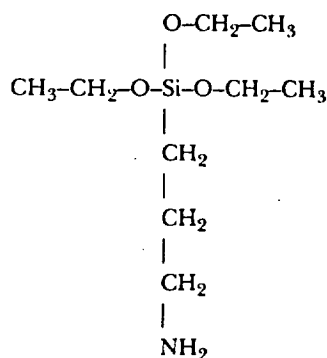
Materials

The disks used were made of 440C stainless steel with a Rockwell hardness of C-57 to C-59. The disks were lapped and polished to a surface finish of 0.040 ± 0.015 µm centerline average (CLA). Instead of using pins, the pin holder was modified to hold 0.476 cm radius (three-eighths inch diameter) commercial grade 10, 440C balls which had the same surface roughness as the disks. The hardness of the balls was Rockwell C-60.

Properties of the PFPE and silane (3-aminopropyltriethoxysilane) liquids used in this study are given in Table 1 and the following are the structures:

The Perfluoropolyalkylether

$$C_3F_7O(-CF-CF_2-O-)nC_2F_5$$
$$|$$
$$CF_3$$

The Silane

$$O-CH_2-CH_3$$
$$|$$
$$CH_3-CH_2-O-Si-O-CH_2-CH_3$$
$$|$$
$$CH_2$$
$$|$$
$$CH_2$$
$$|$$
$$CH_2$$
$$|$$
$$NH_2$$

TABLE 1—PROPERTIES OF PFPE AND SILANE LIQUIDS

PROPERTY	PFPE	ORGANOSILANE
Average Molecular Weight	11,000	221.37
Density (g/cm³)	1.92 (20°C)	0.941 (20°C)
Refractive Index	<1.3 (20°C)	1.421 (20°C)
Viscosity (cST)	2717 (20°C)	—
	63 (100°C)	
Vapor Pressure (Torr)	3 310^{-14} (20°C)	—
	1 3^{-9} (100°C)	
Pour Point (°C)	−15	—
Boiling Point (°C)	None	217
Flash Point (°C)	None	104

Friction and Wear Apparatus

The pin-on-disk tribometer used in this study, shown in Fig. 1, has been described in detail in Ref. (14). The specimens consisted of a flat rotating disk (6.3 cm diameter) in sliding contact with a stationary pin (ball) (0.476 cm radius) which was securely fastened in a holder. The ball slid on disk tracks that ranged from 4.8 cm to 3.7 cm in diameter. The rotational speed of the disk was controlled at 200 rpm giving linear sliding speeds of 0.50 to 0.39 m/s. The test specimens were encased in a plastic box to control the atmospheric humidity. A load of 2 kg was applied to the ball, which gave an initial maximum contact stress of 1.3 GPa (190,000 psi). A polyethylene ring was fastened around the diameter and extended approximately 0.4 cm above the surface of the disk to restrain the oil from being thrown from the disk by centrifugal forces. The amount of oil used for each test was 2 g.

Surface Cleaning

The ball and disk cleaning procedure was as follows:

1. Wash surfaces with ethyl alcohol.
2. Rub surfaces with a water paste of polishing alumina (particle size 0.3 µm). Clean until water readily wetted the surfaces.
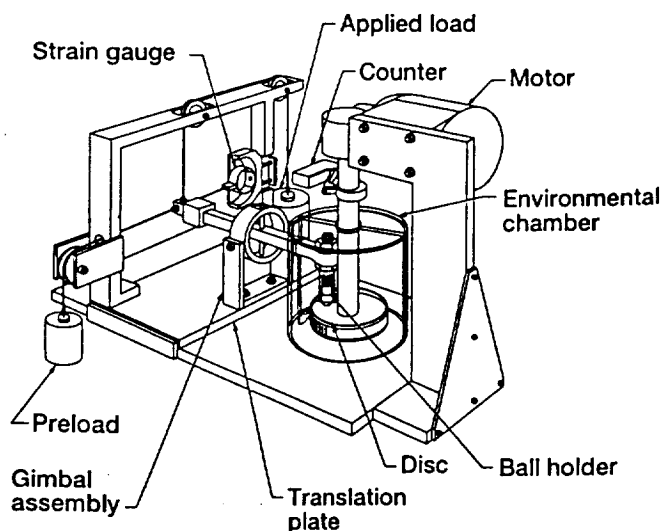3. Scrub surfaces under running tap water with a brush to remove alumina.

Fig. 1—Pin-on-disk tester.

4. Rinse in deionized water.

5. Dry surfaces by blowing on with clean compressed air.

Emulsion Preparation

A one percent (by weight) emulsion of the silane was prepared by first adding the appropriate amount of the silane to the PFPE in a test tube. Since the silane was insoluble in the PFPE, the test tube was placed in an ultrasonic cleaner for 10 minutes to mix the two liquids. The ultrasonic agitation caused the formation of a milky white emulsion.

Coating Application

A one percent (by weight) of the silane in a methanol solution was prepared by adding the appropriate amount of the silane to 100 ml of methanol in a 500 ml beaker. A polished 440C disk was then immersed into this solution for 15 minutes. The disk was carefully withdrawn, placed inside a petri dish and then covered. The covered petri dish was then placed inside a furnace (maintained at 200°C) for 30 minutes. This method produced a coating approximately 3 μm thick.

Emulsion Stability Testing

A small quantity of the emulsion was poured into a sample bottle, sealed, and left to stand for two months. Periodic visual inspection was conducted to check for separation. In addition, a small quantity of the emulsion was placed in a centrifuge and spun at 2500 rpm at a radius of 10 cm for 10 minutes. In an additional test, some of the emulsion was heated in glassware at 250°C for 30 minutes under a partial vacuum (<5 Torr).

Thermal Gravimetric Analysis Testing

Thermal gravimetric analysis (TGA) tests were conducted on the pure PFPE, the silane and the mixture. A small quantity of each liquid was injected onto an aluminum pan, and the pan was then loaded and sealed (under a flowing N_2 atmosphere at 60 ml/min) inside the TGA system. The TGA temperature was ramped at a rate of 10°C per minute from room temperature to 360°C.

Friction and Wear Testing

Two grams of oil (with or without the emulsion) were applied to the disk (with attached polyethylene ring). The ball (securely fastened in its holder) and disk were inserted into the friction and wear apparatus and properly aligned. The test chamber was then sealed and purged with dry air (100 ppm moisture content) for 15 minutes before commencing the tests. This purge was continued throughout the tests. After the 15-minute purge, the disk was set into rotation at 200 rpm and a two-kilogram load was gradually applied to the ball. The test temperature was 25°C.

Each test was stopped after one kilocycle (kc) of sliding. At 200 rpm this is five minutes. The ball holder was removed from the apparatus and the wear area on the ball was examined by optical microscopy and a wear measurement was made. The holder was then placed back into the apparatus and the previous test procedure was repeated. The ball was not removed from its holder, and locating marks insured that the holder was returned to its original position.

Each test was stopped and the above procedure was repeated after sliding intervals of 3, 7, 15, 30 and 50 kc of sliding. Some tests were terminated at this point and some tests were continued for long-duration sliding effects. The long-duration tests were run continuously for up to two weeks (4300 kc or 500 km), being stopped once a day (or after the weekend) to examine the ball wear scars and measure wear. Disk wear tracks were examined by optical microscopy after the tests were terminated (either 50 kc or the long-duration tests).

To determine the friction and wear protection of the silane coating in a stand-alone condition, some tests were conducted on the silane coating without using any PFPE lubricant. Similar testing conditions were applied.

Data Analysis

The data analysis was performed by first entering the distance and wear volume for every sliding interval for each test into a computer spreadsheet. Short-term data analysis considered data taken from the start of the test up to 5000 m of sliding. Five data points were typically recorded in this period. A least-squares regression fit, which was forced to intersect the origin, was used to determine the short-term wear rate for each test. Tests were grouped by treatment type and the mean, maximum, minimum and standard deviation values were calculated.

Long-term data analysis was conducted using a similar procedure except that only data collected between 25 km of sliding and the end of the test were considered. The least-squares regression fit in this case was not forced to intersect the origin for the determination of the long-term wear rates. The same statistics were calculated for each group of long-term tests.

Sliding Surfaces Analysis

Optical microscopy techniques were used to study the lubrication films, the transfer films, and wear debris. The surfaces were viewed at magnifications to 1000.

A μFTIR microscope was also used to observe selected wear surfaces after either 50 kc of sliding or after the long-duration tests (~4300 kc). For information about the operation and use of this spectrometer, see Refs. (15)–(17). The observations were done in the reflectance mode. A gold-coated glass slide was used as a background and the area of analysis was a 100 μm-diameter circle. The ball and disk wear areas were at least 300 μm wide; therefore, several spots within the track were analyzed in order to obtain a better perspective of the surface composition. For comparison, off wear scar areas were also analyzed. Before commencing the μFTIR analysis, the specimens were rinsed with Freon™ and then cleaned in an ultrasonic cleaner to remove excess lubricant in order to obtain access to the deposits on the surface interface. A surface profilometer was also used to examine the cleaned disk wear surfaces.

RESULTS AND DISCUSSION

Emulsion Stability Tests

Visual inspection of the silane/PFPE emulsion that was left to stand for two months on a shelf revealed the persistence

of a milky white color, indicating that the two constituents did not separate. In addition, no separation of the two materials was found to occur in centrifuge testing at 2500 rpm for 10 minutes. Because of these tests, the emulsion was judged to be exceptionally stable.

TGA testing of the emulsion and each constituent was also conducted. Figure 2 shows the results. The TGA thermogram for the pure silane, see Fig. 2(a), showed that nearly all the silane had evaporated by 140°C, whereas the TGA thermogram for the pure PFPE, see Fig. 2(b), showed that the PFPE started to evaporate at about 270°C. The TGA thermogram for the emulsion was the same as that of the pure PFPE in Fig. 2(b). There was no evidence of silane evaporation from the emulsion in the TGA tests; however, the amount of silane present may have been too small to detect.

Because of the TGA results, it was decided to subject the emulsion to a temperature that was higher than the boiling point of the silane but lower than that of the PFPE. Thus, the emulsion was heated under a partial vacuum to 250°C, held at temperature for 30 minutes and then cooled to room temperature. The emulsion still maintained its milky white color and no separation could be observed, indicating no evaporation of the silane had occurred. Vapor pressure measurements of the pure liquids and the emulsion will be conducted in the future to supplement the current work.

Ball Wear

Ball wear was evaluated for sliding distances of up to 4300 kc of sliding (500 km). To determine if there were differences between short-term and long-term effects, wear rates were calculated and compared for two sliding intervals: 0 to 30 kc (0 to 4.5 km) and 50 to 4300 kc (7.5 to 500 km). The
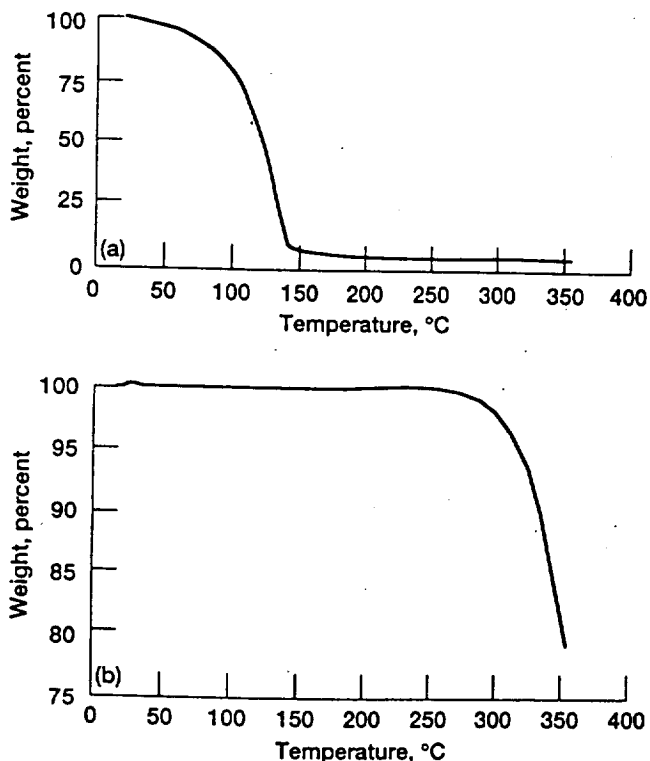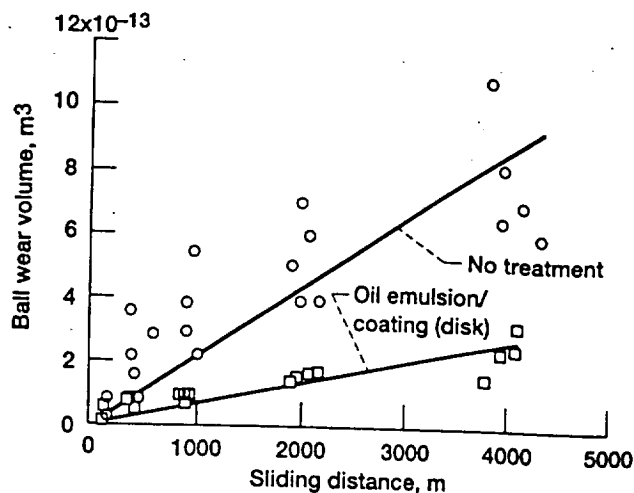
Fig. 3—Ball wear volume as a function of sliding distance for all the tests conducted on a PFPE oil with no silane treatment and for all tests conducted on the same PFPE oil treated with a silane emulsion and a disk coating. The lines shown represent least-squares regression fits of the data which was forced to intersect the origin.

wear as a function of sliding distance for any one particular test was nearly linear during these two sliding intervals and, thus, wear rates were calculated for each test using a least-squares data fit.

Figure 3 shows the experimental data and a least-squares fit for the first 4500 meters of sliding for the lubricant conditions of silane emulsion and silane disk coating and no treatment. Besides having a lower wear rate, much less data scatter was obtained for the oil emulsion/disk coating condition as compared to the no treatment condition. The median ball wear rate results for all the test conditions are shown in Table 2. The table also lists the number of tests conducted under each condition, and the maximum, minimum, and standard deviation of the ball wear rates. Figure 4 gives a comparison of the median pin wear rates and the data scatter for the short-term tests and long-term tests.

For the short-term tests, it was found that the silane decreased the pin wear rate by an average of approximately 50 percent. There did not seem to be any clear advantage of coatings over emulsions or of combining coatings with emulsions. However, it should be emphasized that neither the coatings nor the emulsions were optimized in this study.

In general, ball wear rates were lower for the long-term tests than for the short-term tests, which could be due to run-in effects. In addition, the silane did not decrease the ball wear as much for the long-term tests as it did for the short-term tests. A possible reason for this is that some form of mixed lubrication may be taking place. The authors have observed in unpublished data on accelerated testing devices (such as pin-on-disk and rub-shoe devices where there is 100 percent sliding) that, as the wear scar gets larger, the wear rate decreases. Also, at some point, enough pressure is generated by the liquid to cause complete separation of the surfaces. When this happens, no further wear of the surfaces occurs. Mixed lubrication may be happening in these tests. The silane would not be expected to have as much beneficial effect in mixed lubrication as in pure boundary lubrication.

Fig. 2—Thermogravometric thermograms.
(a) liquid silane
(b) PFPE

TABLE 2—COMPARISON OF BALL WEAR RATES FOR SHORT- AND LONG-DURATION TESTS										
OIL, DISK OR BALL TREATMENT	SHORT-TERM TESTS (0 to 30 kc)					LONG-TERM TESTS (50 to 4500 kc)				
	NUMBER OF TESTS	PIN WEAR RATE (m³/m)				NUMBER OF TESTS	PIN WEAR RATE (m³/m)			
		MAXIMUM	MINIMUM	MEDIAN	STANDARD DEVIATION		MAXIMUM	MINIMUM	MEDIAN	STANDARD DEVIATION
None	6	455×10^{-18}	131×10^{-18}	240×10^{-18}	120×10^{-18}	7	90×10^{-18}	23×10^{-18}	48×10^{-18}	31×10^{-18}
Oil Emulsion	6	129	21	81	36	4	45	21	31	13
Coating (Disk)	8	139	34	84	34	6	49	15	27	12
Coating (Disk and Ball)	3	134	62	91	38	2	18	9	14	6
Oil Emulsion/ Coating (Disk)	4	79	51	65	12	4	29	10	21	8
Oil Emulsion/ Coating (Disk and Ball)	2	120	93	107	19	2	16	9	12	5

Experimental Conditions: Temperature, 25°C; dry air atmosphere (100 ppm moisture content); load, 2 kg; speed, 200 rpm; 440C stainless steel specimens.
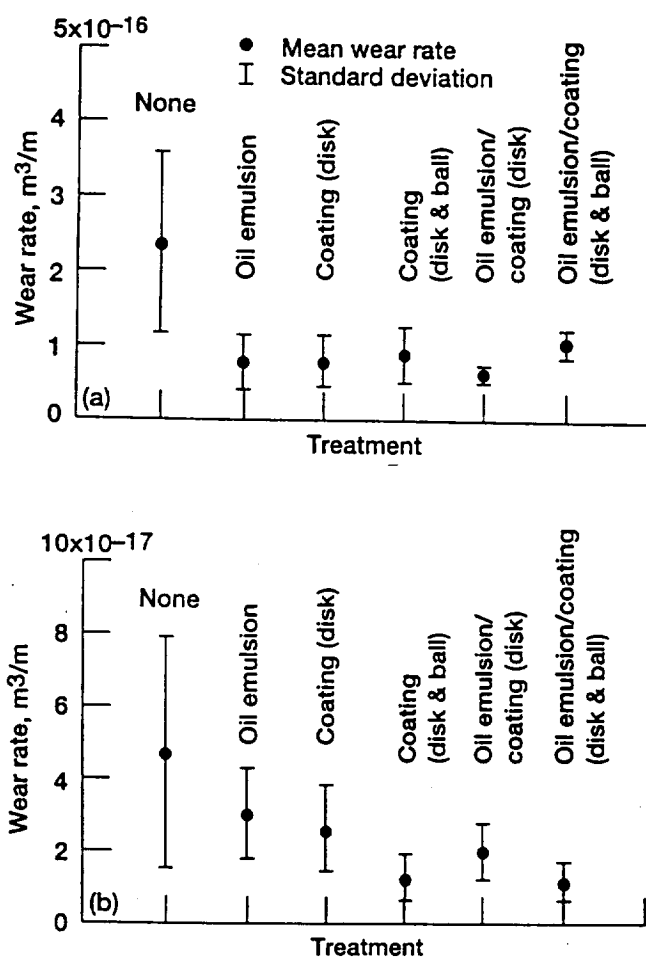

Fig. 4—Comparison of mean ball wear rates and standard deviations.
(a) short-term tests
(b) long-term tests

Coefficient of Friction

The friction results are presented in Table 3. In general, no distinguishable effect on friction coefficient was found which was dependent on either the silane emulsion or the silane coating. The maximum, minimum and median friction coefficients obtained were essentially the same for all experimental conditions. Variation from test to test under any one particular experimental condition was found to differ as much as the variation from adding a silane emulsion or a silane coating. Table 3 also presents the friction coefficient of a silane coating (run dry under the same conditions) for comparison purposes. In the dry condition, the silane coating lasted less than 0.75 km (5 kc) of sliding.

Optical Microscopy

A comparison of the ball wear surfaces after 2 km of sliding is shown in Fig. 5 for the following tests: a silane emulsion, a silane disk coating, and no treatment. For both the silane emulsion and silane coating tests, a much smoother wear scar was obtained and FTIR analysis indicated a deposit of silane was adhering to the wear scar. The ball scar from the test with no silane treatment showed a very rough surface, much more black powdery wear debris and some plastic deformation of the scar in the exit region.

Figure 6 compares the wear tracks on 440C stainless steel disks after very long durations of sliding under three different PFPE lubricant conditions. Shown in the figure are a disk track with a silane emulsion and coating after 250 km of sliding, a disk track with a silane coating after 237 km of sliding, and a disk track with no silane treatment after 230 km of sliding. The disk track lubricated with PFPE with no treatment shows a large amount of black powdery wear debris (especially in the center of the track). The silane-coated disk shows a dark material on the wear track that appears to be platelet-like. The silane emulsion shows a disk wear track that has nearly no visible deposits.

Photomicrographs of the ball wear surfaces were also taken after long durations of sliding. Figure 7 shows a low and high magnification photomicrograph of a ball wear scar after 350 km of sliding where the counterface was a silane-coated 440C stainless steel disk. The ball wear scar is seen to be very smooth and the transfer is thin and "platelet-like." μFTIR analysis of this scar showed that the transfer contained silane. Figure 8 shows a photomicrograph of a ball wear scar after 266 km of sliding where no silane emulsions or coatings to

OIL, DISK OR BALL TREATMENT	SHORT-TERM TESTS (0 to 30 kc)				LONG-TERM TESTS (50 to 4500 kc)			
	NUMBER OF TESTS	FRICTION COEFFICIENT			NUMBER OF TESTS	FRICTION COEFFICIENT		
		MAXIMUM	MINIMUM	MEDIAN		MAXIMUM	MINIMUM	MEDIAN
None	6	0.16	0.09	$0.13 \pm .02$	3	0.17	0.10	$0.14 \pm .02$
Oil Emulsion	6	0.16	0.09	$0.13 \pm .02$	2	0.17	0.11	$0.14 \pm .01$
Coating (Disk)	8	0.16	0.09	$0.14 \pm .02$	5	0.16	0.10	$0.13 \pm .02$
Coating (Disk and Ball)	3	0.17	0.11	$0.14 \pm .01$	2	0.16	0.12	$0.14 \pm .01$
Oil Emulsion/ Coating (Disk)	4	0.16	0.10	$0.13 \pm .02$	4	0.16	0.11	$0.14 \pm .01$
Oil Emulsion/ Coating (Disk and Ball)	2	0.17	0.11	$0.14 \pm .01$	2	0.16	0.13	$0.14 \pm .01$
Dry Silane Coating (No Oil)	2	0.35	0.18	$0.25 \pm .05$	—	—	—	—

TABLE 3—COMPARISON OF FRICTION COEFFICIENTS FOR SHORT- AND LONG-DURATION TESTS

Experimental Conditions: Temperature, 25°C; dry air atmosphere (100 ppm moisture content); load, 2 kg; speed, 200 rpm; 440C stainless steel specimens.

the disk were employed. Dark powdery transfer is observed as well as an area where the oil is not wetting the surface. It is not certain why this phenomena occurred, but this de-wetting phenomena has been observed using the PFPE lubricants on other occasions by the authors. The dewetting phenomena was not observed for any test in which silane was used as an additive or as an emulsion.

Disk Surface Profilometry

Figure 9 compares the disk wear track areas after 50 kc of sliding for PFPE oil with a silane emulsion and for a PFPE oil with no treatment. The wear track area for the test with the silane emulsion has a cross-sectional area of 59×10^{-12} m^2, while the test without the silane had a wear track with a cross-sectional area of 214×10^{-12} m^2.

Micro-Fourier Transformation Infrared Spectroscopy

A comparison of the μFTIR spectrum of the PFPE film on a 440C disk wear track before testing (dotted line) to the μFTIR spectrum of the PFPE fluid on the same wear track after it had been treated for 50 kc (solid line) is shown in Fig. 10. The multiple-featured C-F peak between 1100 and 1400 cm^{-1} and the sharp CF_3 peak at 980 cm^{-1}, which corresponds to the CF_3 rotation-vibration, are characteristic of this particular PFPE lubricant. The peak in the 3000 to 3500 cm^{-1} region is due to H-bonded -OH. The broad peak at 1670 cm^{-1} and the small peak at 1425 cm^{-1}, which overlaps the water vibrations, could be due to two types of structures. Liang and Roselius (18) suggested that the degradation products on the surface have a structure of perfluoroacyl-fluoride bounded to the surface through a hydroxyl. Thus, the peak at 1670 cm^{-1} could correspond to a C=O vibration, and the 1425 cm^{-1} peak would then correspond to the end C-F vibration. The second possibility is the formation of a surface carboxylate, COO^{8-}, formed by the reaction of a perfluoroacylfluoride with a surface or ambient water. At the present time, there is not enough spectroscopic evidence to discern which is the correct structure. However, there is

enough evidence to definitely state that the observed μFTIR spectra corresponded to the signature of the degraded lubricant.

To ascertain if silane were transferred from the emulsion or coating to the mating surfaces, a μFTIR spectrum of the silane coating was taken before testing and then compared to deposits on the ball wear surfaces. Figure 11 shows the μFTIR spectrum of the silane coating applied to a 440C steel surface. The two sharp bands at 3367 and 3298 cm^{-1} are typical N-H asymmetric and symmetric stretching vibrations which occur in NH_2 groups. The band at 1600 cm^{-1} is the corresponding deformation vibration. Hydrogen bonding is typical in the solid or liquid state for compounds containing NH_2 groups. Thus, hydrogen bonding accounts for the broad peak between 3000 and 3500 cm^{-1}. Since this film has been baked after its application to the 440C surface, it is unlikely that this broad vibration would be due to H-bonding of hydroxyl groups. Other peaks present are the C-H stretching vibrations due to the C_2H_5 and the C_3H_6 groups which appear at 2840 and 2932 cm^{-1}, respectively. The band at 1470 cm^{-1} is the corresponding deformation vibration. The Si-O-C_2H_5 vibrations appear at 1100 and 930 cm^{-1} and the Si-C_3H_6 appear at 792 cm^{-1}.

Figure 12 compares the μFTIR spectra in the 5000 to 1500 cm^{-1} wavenumber region from spectra taken from wear scars which were slid against silane-coated disks. Spectra are shown for a short-duration test (50 kc) and for a long-duration test (4300 kc). The spectrum for the short-duration test shows the presence of silane peaks (C-H and N-H vibrations) but does not show any PFPE decomposition peaks (-OH and C=O vibrations). The long-duration spectrum shows no silane peaks but does show the presence of PFPE decomposition peaks. The -OH vibration (3500 to 3000 cm^{-1}) is very shallow and is somewhat hidden in the broad peak shown on Fig. 12; however, the other degradation signature peak (C=O vibration) is very visible on the figure at 1625 cm^{-1}. The presence of silane peaks on the surface and the absence of decomposition peaks (after the short sliding interval) strongly infer
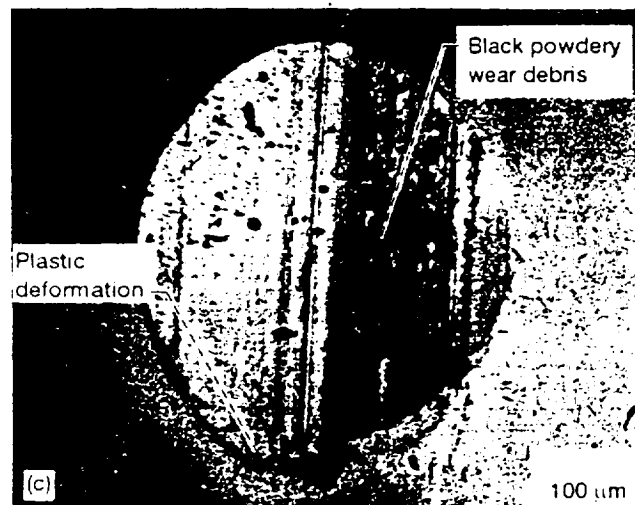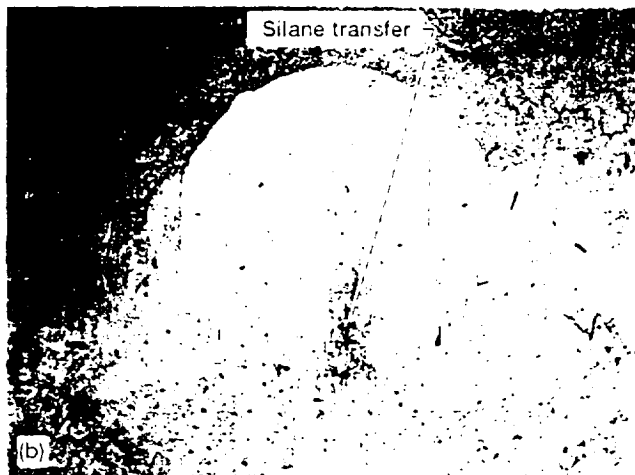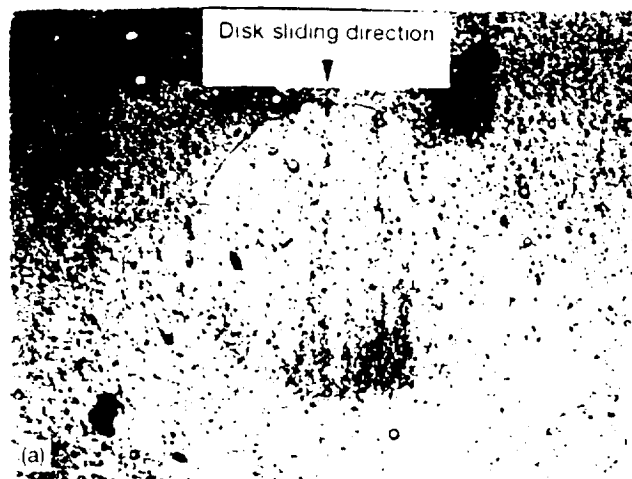
Fig. 5—Comparison of ball wear scars after 2 km of sliding.
  (a) silane emulsion
  (b) silane disk coating
  (c) no silane treatment
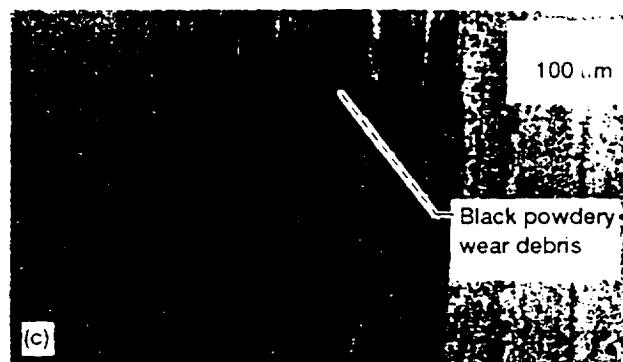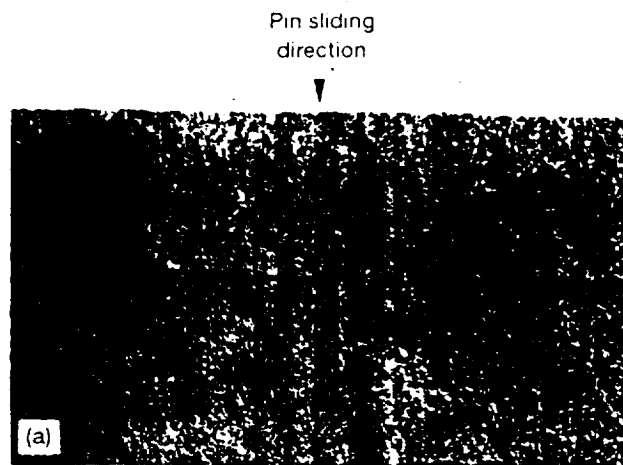

Fig. 6—Comparison of wear tracks on 440C stainless steel disks after very long durations of sliding.
  (a) silane emulsion and coating (250 km)
  (b) silane disk coating (237 km)
  (c) no silane treatment (230 km)

that the silane has helped mitigate the degradation of the PFPE. The absence of silane peaks (after the long sliding duration) indicates that the silane coating eventually wears away.

All the tests using silane showed a reduction in degradation of the PFPE lubricant for the short sliding durations. However, no silane peaks could be found on the wear surfaces for the tests using the silane emulsion. It may be that the

interaction of the silane in this case took place between the PFPE and the silane and that transfer of the silane to the wear surfaces was not necessary to prevent degradation.

CONCLUDING REMARKS

The purpose of this study was to determine if a silane added to a PFPE as an emulsion or applied as a coating to the counterfaces would reduce wear and/or the degradation of a PFPE lubricant. It was found that both wear and degradation were reduced. The authors believe that reduced degradation of the lubricant leads to reduced wear, although there is no experimental proof of this.

In addition, it is important to bear in mind that no attempt has been made in this study to optimize the method of ap-
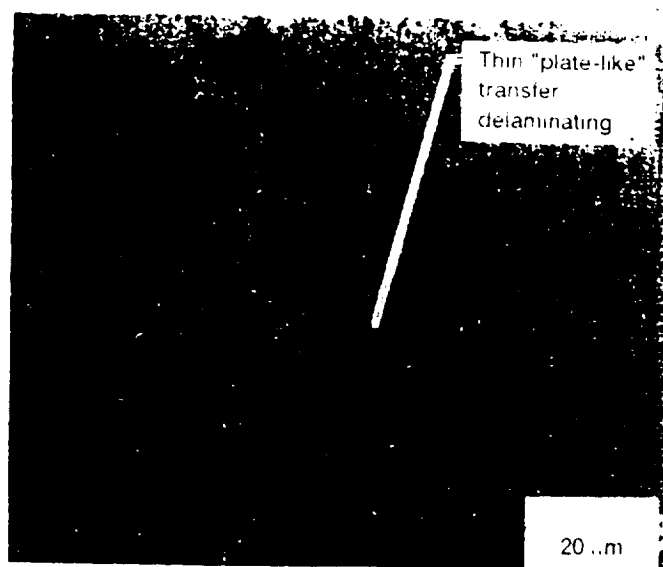
Fig. 7—Low and high magnification photomicrographs of ball wear scar areas after 350 km of sliding from a test where the counterface was a silane-coated 440C stainless steel disk.
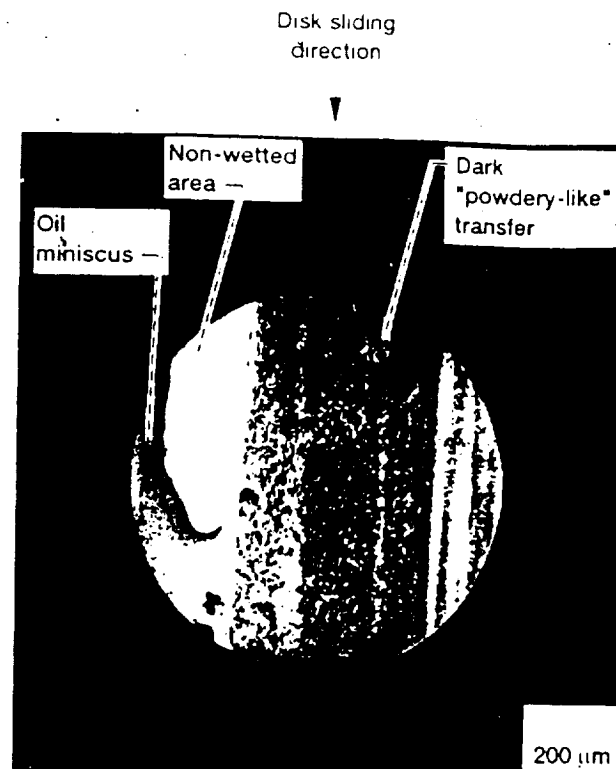

Fig. 8—Photomicrograph of a ball wear scar after 266 km of sliding from a test where no silane emulsions or coatings to the disk were employed. Dewetting of the oil from the surface can be observed.
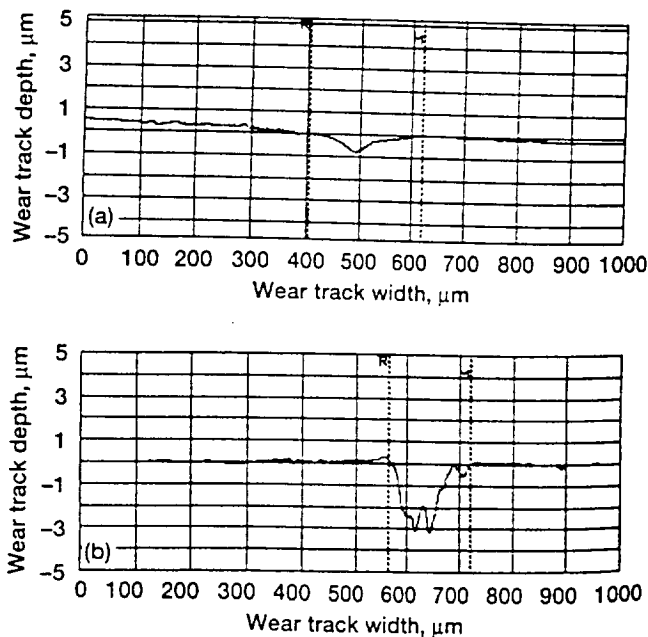

Fig. 9—Comparison of disk wear track cross-sectional areas after 50 k: of sliding for tests conducted in various conditions.
(a) a PFPE oil with a silane dispersion
(b) a PFPE oil with no silane dispersion or coating

plying the coatings, the thickness of the coatings, the curing of the coatings, or the amount of the silane in the emulsion. Thus, it may be possible to obtain even better results once an optimization study is done. It also should be noted that the silane emulsions and coatings are not necessarily the same. The emulsions were not heat treated while the coatings were heat treated at 200°C for 30 minutes. Heat treating of the silane may have changed its structure.

Also, one must be aware that accelerated test data such as wear rates, friction coefficients, etc. do not necessarily directly correlate to results achieved in an actual bearing. A

very small improvement in an accelerated test data may lead to a very large improvement in a bearing or there may be very little improvement. A test using bearings must be made to ascertain the real improvement. Screening tests, such as pin-on-disk tests, are done to show the potential of various concepts for use in a bearing.
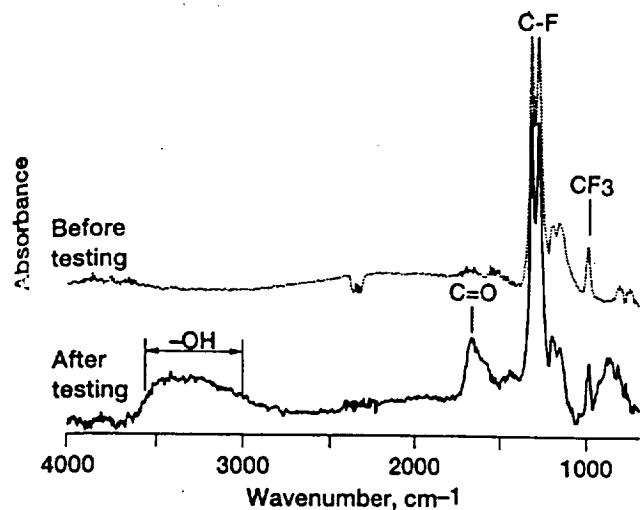
Fig. 10—Comparison of FTIR spectra of PFPE oil on a 440C stainless steel ball before testing to that obtained on the 440C steel ball wear scar after 50 kilocycles of sliding (no treatment of the oil).
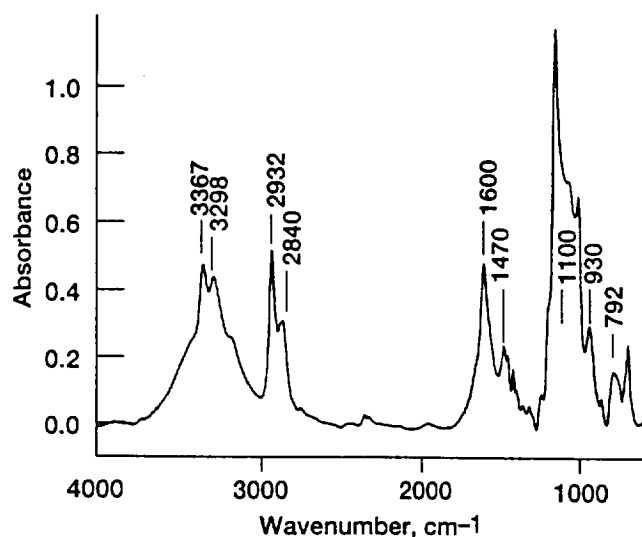

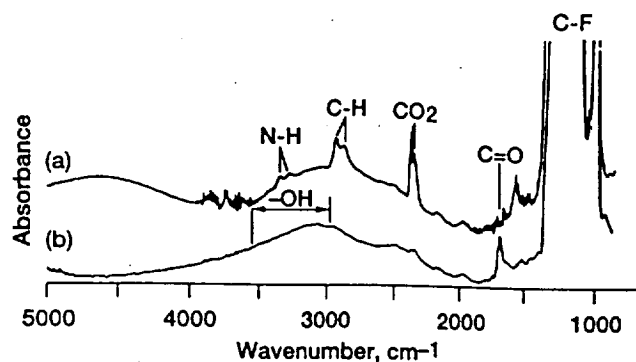Fig. 11—FTIR spectra of a silane coating applied to a 440C stainless steel disk.

Fig. 12—Comparison of FTIR spectra obtained from ball deposits on the wear scar after various durations of sliding on a silane-coated disk (-OH and C=O are PFPE decomposition peaks, N-H and C-H are silane peaks).
(a) 50 kilocycles
(b) 4300 kilocycles

that the silane disk coatings could form thin layerlike transfer films on ball wear surfaces.

5. Friction coefficients obtained from PFPE oil tests using silane emulsions or silane coatings were the same as those obtained from tests using the untreated PFPE oil.

SUMMARY OF RESULTS

Pin-on-disk tribology testing coupled with surface profilometry, optical microscopy and µFTIR studies on a PFPE liquid lubricant with and without silane additives and/or emulsions provides the following indications:

1. Silane coatings and/or emulsions used in conjunction with PFPE oils eliminated PFPE degradation products which were found on ball wear surfaces on tests with the untreated oil, giving strong evidence that the silane can mitigate the degradation of this particular PFPE oil.
2. Accompanying the reduced degradation of the PFPE oil was reduced wear of 440C balls and disks when compared to similar tests on an untreated PFPE oil.
3. Equal improvements in decreased wear rates were obtained for disk coatings and oil emulsions, although no attempt was made to optimize either application method.
4. Optical and µFTIR microscopy observations indicated

REFERENCES

(1) Gumprecht, W. H., "PR-143—A New Class of High Temperature Fluids," ASLE Trans., 9, pp 24–30, (1966).
(2) Sianesi, D., "Perfluoropolyalkylethers Synthesis and Characterization of a New Class of Inert Fluids," Chim Ind. (Milan), 50, p 206, (1968).
(3) Holland, L., Laurenson, L. and Baker, P. N., "The Use of Perfluoropolyether Fluids in Vapour Stream Pumps," Vacuum, 22, p 315, (1972).
(4) Luches, A. and Provenzano, I., "On the Use of Perfluoropolyether Fluids in HV Spark-Gaps," Jour. Phys. D: Appl. Phys., 10, pp 339–342, (1977).
(5) Sianesi, D., Zamboni, V., Fontanelli, R. and Binaghi, M., "Perfluoropolyethers: Their Physical Properties and Behaviour at High and Low Temperatures," Wear, 18, pp 85–100, (1971).
(6) Sharma, S. K., Gschwender, L. J. and Snyder, C. E. Jr., "Development of a Soluble Lubricity Additive for Perfluoropolyalkylether Fluids," Jour. of Synth. Lubr., 7, 1, pp 15–23, (1990).
(7) Gschwender, L. J., Snyder, C. E. Jr. and Fultz, G. W., "Soluble Additives for Perfluoropolyalkylether Liquid Lubricants," Lubr. Eng., 49, 9, pp 702–708, (1993).
(8) Carré, D. J. and Markowitz, J. A., "The Reaction of PFPE Oil with FeF₃, AlF₃, and AlCl₃ at Elevated Temperatures," ASLE Trans., 28, 1, pp 40–46, (1985).
(9) Zehe, M. J. and Faut, O. D., "Acidic Attack of PFPE Lubricant Molecules by Metal Oxide Surfaces," NASA TM—101962, (1993).
(10) Kasai, P. H., Tang, W. T. and Wheeler, P. O., "Degradation of PFPEs Catalyzed by Aluminum Oxide," Appl. Surf. Sci., 51, pp 201–211, (1991).
(11) Basu, P., Ballinger, T. H. and Yates, J. T. Jr., "Fluoroalkyl Ether Chemistry on Alumina: A Transmission IR Study of the Adsorption and Thermal Decomposition of (CF₂H)₂O on Al₂O₃," Langmuir, 5, 2, pp 502–510 (1989).
(12) Ng, L. M., Lyth, E., Zeller, M. V. and Boyd, D. L., "Surface Chemistry of Perfluoro Ethers: An Infrared Study of the Thermal Decomposition of (C₂F₅)₂O on Al₂O₃," Langmuir, pp 127–135, (1995).
(13) Morales, W., "Perfluoropolyalkylether Decomposition on Catalytic Aluminas," NASA TM 106547, (1994).
(14) Fusaro, R. L., "How to Evaluate Solid-Lubricant Films Using a Pin-on-Disk Tribometer," Lubr. Eng., 43, 5, pp 330–338, (1987).
(15) Hollis, P., "Surface Infrared Spectroscopy," Vacuum, 45, pp 705–714, (1994).
(16) Porter, M. D., "IR External Reflection Spectroscopy: A Probe for Chemically Modified Surfaces," Analytical Chem., 60, pp 1143A–1155A, (1988).
(17) Reffner, J. A., "Infrared Microanalysis of Contaminants at Grazing Incidence," Appl. Spectroscopy in Mat'l. Sci., 1437, pp 89–94, (1991).
(18) Liang, J. and Roselius, M., "FTIR Study of Perfluoroacyl Fluoride Chemisorption onto Alumina," Jour. of Fluorine Chem., 67, pp 113–117, (1994).